Strojniški vestnik - Journal of Mechanical Engineering 54(2008)10, 662-674
UDC 621.63

Paper received: 10.01.2008
Paper accepted: 07.07.2008

Impact of the Guard Grill on the Integral and Local Characteristics of an Axial Fan

Gregor Ališ [1,*] - Brane Širok[2] - Vlado Schweiger[1]
[1] Institute Hidria Klima, Godovič, Slovenia
[2] University of Ljubljana, Faculty of Mechanical Engineering, Slovenia

This paper presents the impact of the guard grill (GG) on the integral characteristic (IC) and local aerodynamic properties of the outflow of an axial fan (AF). The study of the GG's impact was conducted using measurements and numeric modelling at the integral and local levels. Measurements of IC were performed according to the ISO 5801 standard and the local velocity field was measured by using a five-hole probe. Numeric simulations of the machine's local characteristics were made in the same working conditions of the fan. The comparison of results was used in the analysis of the GG's impact on the fan's efficiency and in the analysis of the feasibility of the CFD modelling of flow conditions of the GG.

Keywords: axial flow fans, guard grids, integral characteristic, velocity fields

0 INTRODUCTION

In industrial practice the development of an AF is mostly performed on the assumption of the decisive impact of the rotor and the inlet of the fan on operating conditions, while the impact of the GG and the supporting construction is empirically evaluated or ignored. No research has yet been performed on the GG's actual impact and the supporting construction of the AF on the precise determining of the fan's operating characteristics and outflow kinematics.

Eck [2] and [3] presented the analytical procedures of designing axial and centrifugal fans, while Wallis [1] discuss the analytical procedures for designing AF together with inlet and outlet channels. The programming and analytical design of a fan based on a similar basis as described in the literature [1] to [3] was given by Zhou Dugao et al. where the results of the fan's optimisation were also presented [17]. A common feature of the presented literature [1] to [3] and [17] is that it fails to take into account the impact of the GG on operating characteristics. Several papers have also been written on experimental and numerical studies of flow conditions in the AF. The paper by Yang Li et al. [4], studying the impact of the direction of the blade curvature of similar fans on IC and by five-hole probe and hot wire anemometry the impact on the local vector velocity field, represents the basis for the experimental procedures used in the presented paper. Studies of local kinematics in the flow field of the AF are also discussed in papers [5] with hot wire anemometry [6], with laser Doppler anemometry [9] and [10], computer visualisation and [7] and [8] numeric modelling which reveals the extensive research in this field.

The significance of the GG's impact on the IC of the fan is also evident from the number of patents related to its design [12] to [14]. The question arises of the characteristics of the impact of the GG on the IC of the AF and on the flow kinematics in the flow tract of the fan. Further on, the paper focuses on the GG's impact through a numeric and experimental approach and presents the feasibility of evaluating the impact of the GG on the IC of the fan.

0.1 Description of the Fan with and without the Guard Grill

The analysis of the GG's impact on the fan's characteristics was performed on the AF with seven unprofiled blades curved forward. The basic geometrical characteristics of the fan were given by: diameter of the outlet D_{max} = 510 mm and the dimensionless hub to tip R_{pe}/R_{ob} = 0.28. The fan with the GG is presented in Fig. 1 with characteristic ratia adjusted to the maximum radius of the fan's rotor: distance of the GG from the outlet area to the outlet radius s/R_{max} = 0.235, with the start of the rectangular area of the GG to the axis of rotation at s/R_{max} = 0.898 and the end

*Corr. Author's Address: Institute Hidria Klima d.o.o., Godovič 150, 5275 Godovič, Slovenia, gregor.alic@hidria.com

of the rectangular area of the GG to the axis of rotation at $s/R_{max} = 0.592$. A fan with no GG is fixed on the outlet via the supporting construction with four legs as presented in Fig. 2. The deviation of four supporting consoles from the level of fixing the rotor is significantly bigger than the distance of the GG which permits an assessment of the hypothesis that the supporting consoles in Figure 2 do not affect the flow conditions at the outlet from the rotor.

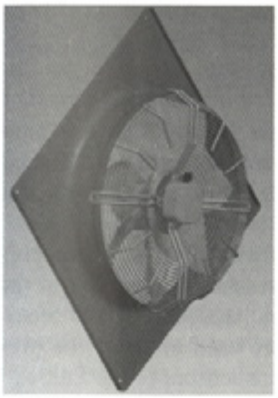

Fig. 1. *Fan with the guard grill*

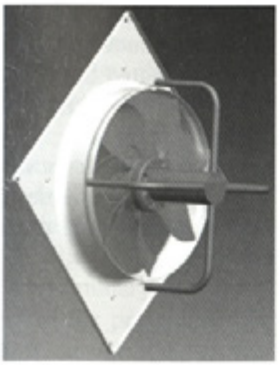

Fig. 2. *Fixing of the fan to the outlet without guard grill*

An experimental comparative study was performed on the presented versions of the AF with regard to the GG's impact on the IC and an experimental and numeric study with regard to the GG's impact on the velocity field at the fan's outlet in the same marginal working conditions.

0.2 Measuring the Integral Characteristics

Integral measurements of the fan with and without the GG were performed at the fan measurement station at the Hidria Institute Klima according to standard ISO 5801, Fig. 3.

The operating characteristics of both fans given as the dependence of pressure difference from the volume airflow on the fan were determined in the entire working range. The volume flow of fans q_V was measured on measurement nozzles with a sensor of differential pressure and static pressure in front of the nozzle. The Mensor 6100 sensor was used in both cases. The static pressure difference Δp at the fan was measured with the same sensor. The Vaisala HMT 330 measuring device for temperature and relative humidity was used to determine the ambient conditions and pertaining air density, while the barometric pressure was measured with the Vaisala PTB 220 measuring device. The connecting electrical power P_{el} and the rotating frequency of the fan's rotor were measured in addition to the aerodynamic parameters. Electrical power was measured with the Zimmer LGM450 digital power analyser and the rotating frequency n was measured with an HIK IJ measuring device. The efficiency of the fan is given by the Equation (1) which, together with the aerodynamic characteristic $\Delta p(q_v, P_{el})$, represents the IC of the fan:

$$\eta = \frac{\Delta p \, q_V}{P_{el}} , \qquad (1)$$

The measurement uncertainty for the volume flow is ±2%, for differential pressure ±1.4% and for electrical power 1% of the measurement range. As the measurement procedures and measuring equipment used did not change for either of the two tested fans, we can assume that the measurement uncertainty was the same in both cases.

0.3 Description of Measuring the Local Velocity

In order to study the GG's impact on the flow conditions, we later conducted measurements of the outflow from the fan. Measurements of local velocity were performed using a five-hole probe which is primarily suitable for determining the intensity and direction of a velocity field; however, it is unsuitable for a reliable assessment of the fluctuation characteristics of the velocity field which was not expected in the analysis.

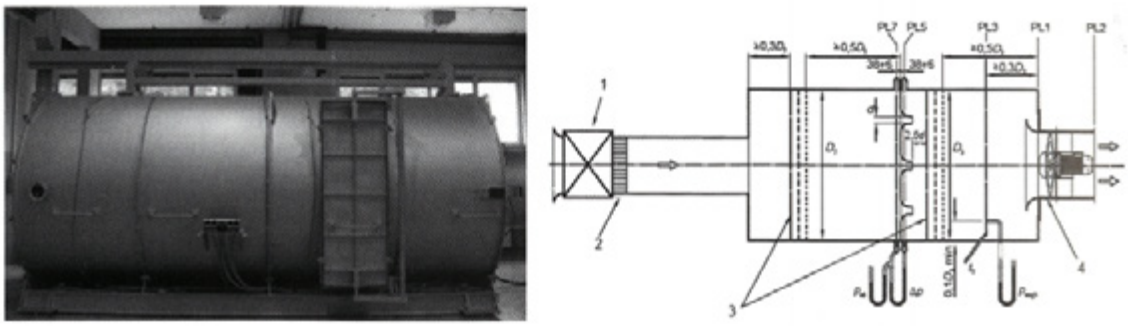

Fig. 3. *Test station for fans made occording to standard ISO 5801 and its section view* [11]
1 – axuliry fan, 2 – flow straightener, 3- seattling mesh, 4-tested fan

Assumptions for the measurement were that the fluid flow is steady for each set working point and that it is symmetrical to the axis of the rotor's rotation.

To meet the condition of axial symmetry, the experiment was conducted in a coaxial channel allowing an unhindered entry and exit velocity field with no swirl flow structures. We provided the on-flow length of $3xR_{max}$, where R is the radius of the entry cylindrical channel, and the free exit of the airflow of the fan in the semi-area with a radius of $4xR_{max}$, in line with the requirements of the ISO 5801 standard. The outline of the station is presented in Figure 4.

Velocity values and the pertaining velocity components were calculated by using ratia of the measured pressure on the five-hole probe, the measured angle α and calibration algorithms of the probe. For this paper, the algorithms were provided by the manufacturer of the five-hole probe, United Sensor. Figure 5 presents the co-ordinate system selected for the experiment and enabling the appropriate presentation of the results.

The differences in static pressure on the individual pressure connections of the probe were acquired simultaneously. PVC tubes of a 5 mm diameter were used to guide the pressure signals to the pressure sensors of the Endres + Hauser PD 235 type. The sampling time interval was identical for all measured points at 60s. The sampling frequency by channel was 100 Hz with 6000 samples per channel. Measuring of each working point was repeated until a dissipation of measured values has fallen under 1.5% of an average measured pressure. The ambient conditions for the measurements determined by the temperature of the environment, barometric pressure and air humidity were measured before each measurement point.

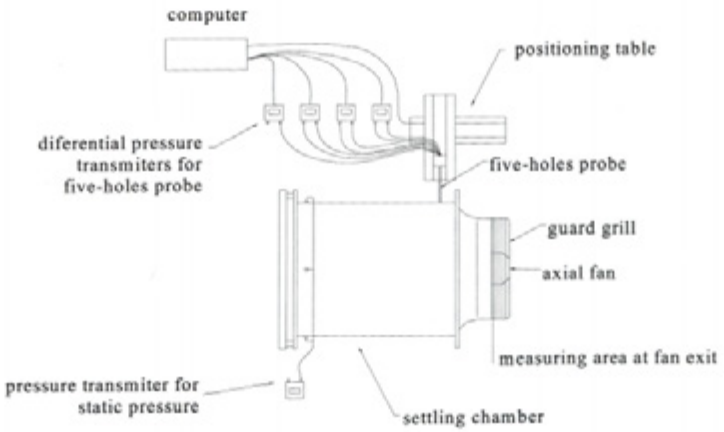

Fig. 4. *Outline of the station for measuring local characteristics with a five-hole probe*

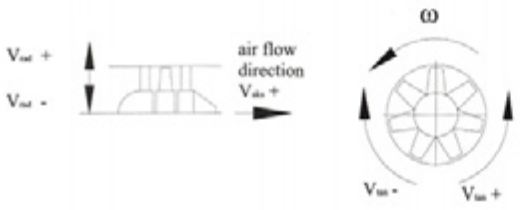

Fig. 5. *Direction of axial v_{aks}, tangential v_{tan} and radial v_{rad} component of velocity vector*

The measuring of the ambient conditions was undertaken in an identical manner and with identical equipment as measurements of the IC.

The overall measurement uncertainty in measuring the velocity by the five-hole probe [15] and [16] depended on the measurement uncertainty of the differential pressure and on average equalled ±3% of the measured value at velocities above 10 m/s [16]. The relative error was increasing with the reduction of velocity, as expected. Given the fact that areas with a smaller velocity were less important for the analysis and that the trend in changes of the velocity field is maintained, we can ignore the increased measurement uncertainty in that area.

The uncertainty of setting the five-hole probe is limited by the uncertainty of the positioning table and setting of the initial point ±1.5 mm.

Measurements of local characteristics were made in three 'stable' working points of the fan on the outlet side of the fan (points A, B and C in the diagram in Figure 8). They were selected on the basis of a preliminary analysis of the integral measurements of the properties of both fans. As the working points at the selected number of revolutions of the fan's rotor were given in couples (q_V, Δp), the selection of the working point

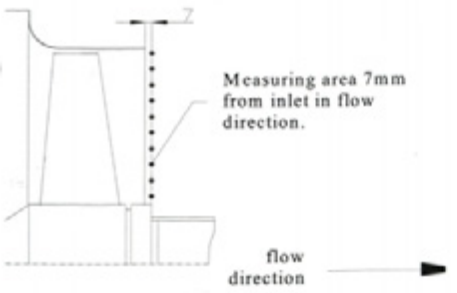

Fig. 6. *Area of outlet velocity measurement with measuring point position*

for local measurements was already determined by the measurement of the pressure difference on the fan to simplify the experiment. Measurements of the local characteristics of the fan with and without the GG were made 7 mm behind the fan's orifice, Figure 6.

Ten measurements were made within the radii ratios r/R_{max} from 0.412 to 0.941 with the step $\Delta r/R_{max}$ 0.059.

0.4 Numeric Model Description

The numeric analysis included a definition of the geometric model, setting up the topological model, Figure 7 and a calculation of the flow field by using the SST (Shear Stress Transport) turbulent model of the software CFX 10.0 with identical marginal conditions as in the measurements.

SST turbulence model used Reynolds averaged Navier-Stokes equations for a steady conditions:

- mass conservation equation, Eq. 2,
- momentum conservation equation, Eq. 3
- along with equations of k-ω SST turbulence model, Eq. 4 and 5 are forming closed system of Eqs [8]:

$$\frac{\partial\left(\overline{u}_j\right)}{x_j} = 0 \tag{2}$$

$$\frac{\partial\left(\rho\overline{u}_j\overline{u}_i\right)}{\partial x_j} = -\frac{\partial\overline{p}}{\partial x_i} + \frac{\partial}{\partial x_j}\left[\mu\left(\frac{\partial\overline{u}_i}{\partial x_j} + \frac{\partial\overline{u}_j}{\partial x_i}\right) - \rho\overline{u_i{}'u_j{}'}\right] \tag{3}$$

$$\frac{\partial\left(\rho k\overline{u}_j\right)}{\partial x_j} = \frac{\partial}{\partial x_j}\left[\Gamma_k\frac{\partial k}{\partial x_j}\right] + \tilde{G}_k - Y_k \tag{4}$$

$$\frac{\partial\left(\rho\omega\overline{u}_j\right)}{\partial x_j} = \frac{\partial}{\partial x_j}\left[\Gamma_\omega\frac{\partial\omega}{\partial x_j}\right] + G_\omega - Y_\omega + D_\omega \tag{5}$$

$\tilde{G}_k$ is the turbulence kinetic energy source, because of velocity gradients, G_ω is the source of ω. Γ_k and Γ_ω are the effective diffusivity of k and ω. Yk and Yk and Yω represent dissipation of k and ω, because of turbulence. Dω is the cross-diffusion term.

The topological model is based on identical assumptions as in the experiment in local measurements of the flow field: the fluid

flow is steady for each calculation point and the fluid flow is axially symmetrical with regard to the axis rotation. Air density was 1.2 kg/m^3 and the dynamic viscosity was 1.79×10^{-5} Pas.

We used those assumptions to establish a topological model with 1/7 segment of the geometric model [8] with a hexagonal grid for the fan with and without the GG, Figure 7, with the specifications presented in Table 1. The assumption in setting the topological grid on the fan with the GG was that the concentric protective wire covering roughly 35% of the available outflow area of the outlet has a much greater impact than the radial supporters of the fan, covering roughly 3% of the available outflow area of the outlet. An identical assumption was made for the fan without the GG, where the radial supporters were further distanced from the outflow outlet by the distance $s_{no}/R_{max} = 0.76$, which is characteristically more than in the case of a GG.

Marginal conditions of the numeric simulation were determined on the basis of the preliminary measurement of the fan's local velocities with and without the GG.

The convergence criterion was set with regard to the development of pressure and mass flow. The convergence criterion was met with a decrease in the average remains of each quantity in the entire calculation domain by $1x10^{-6}$, which required at least 350 iteration steps.

1 MEASUREMENTS AND NUMERIC SIMULATION RESULTS

Below is a presentation of the results of measuring the integral and local characteristics of the fan and results of the numeric model for the fan with and without the GG. A comparison of the results of the experiment and the model is possible on those diagrams where integral and local characteristics were given separately. As regards IC, the analysis of the GG's impact on the fan's characteristics is primarily directed at assessing the GG's impact on the operating characteristic $\Delta p(q_V)$ and efficiency η while at the local level the analysis is directed at the GG's impact on the velocity distribution at the exit of the fan's airflow.

1.1 Integral Characteristic of the Fan

The diagrams in Figs. 8 and 9 present the measured IC of the fan. Values were set to constant a rotational speed of $n = 1392$ rpm and the air density of $\rho = 1.2$ kg/m^3 so that the fans' characteristics with and without the GG are comparable. In identical set conditions the diagram also gives the modelled values (MV) for both version of the fans.

Fig. 7. *Overall and detailed 3D calculation model of fan with the guard grill*

Table 1. *Topological data of the calculation area of fan with and without the guard gril.*

	Fan with the guard grill	**Fan without guard grill**
Number of nodes	832512	527760

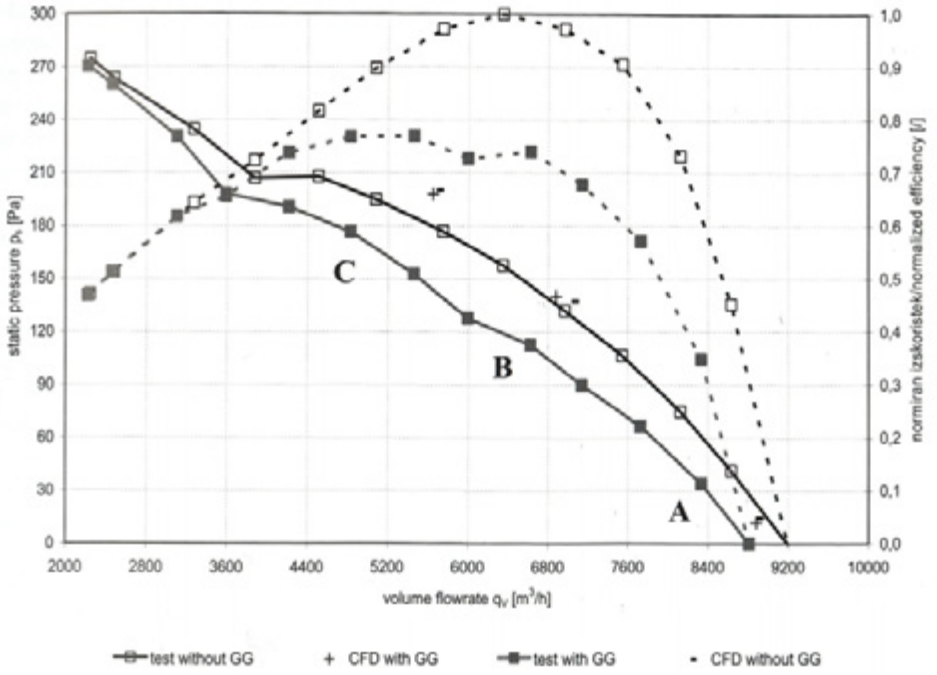

Fig. 8. *Comparison of the integral characteristic differential pressure–flow of fan with and without the guard grill*

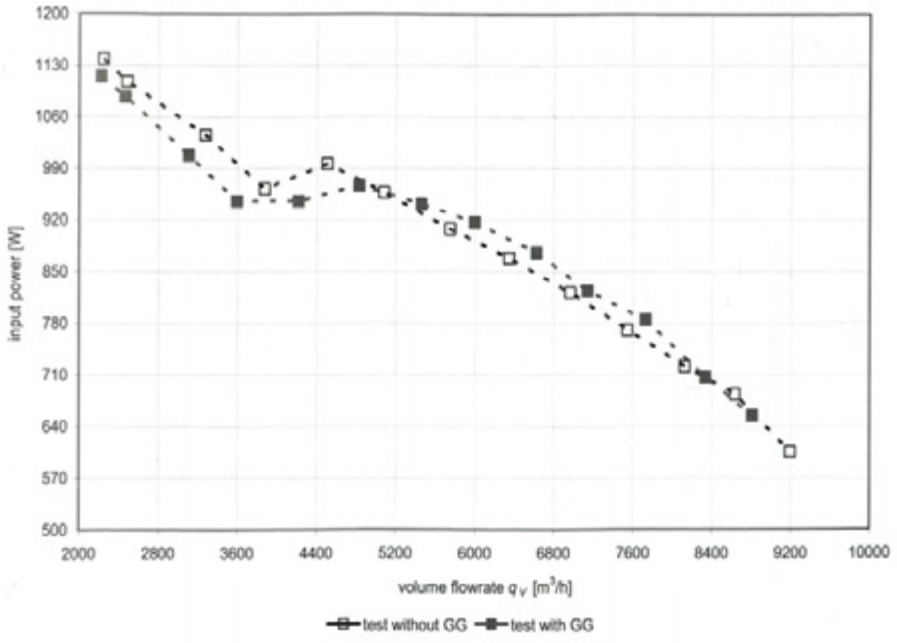

Fig. 9. *Comparison of the integral characteristic electrical power–flow of fan with and without the guard grill*

The abscissa presents the volume airflow q_V, and the ordinates present the static pressure difference Δp and the efficiency of the fan which is set for the maximum efficiency of the machine.

The functional dependence of the static pressure difference from the flow $\Delta p(q_V)$ (the thin full curve) presented in Figure 8 and the dependence of efficiency from the flow $\eta(q_V)$ (the thin dotted curve) enable an assessment of the GG's impact. Figure 5 presents the fan's IC – consumed power-flow $P_{el}(q_V)$ (the dotted curve). Both figures present the characteristics of the fan with the GG marked with full squares and characteristics of the fan without the GG marked with empty squares. The modelled values of the IC of the fans $\Delta p(q_V)$ were given by three points for each version on the fan in Figure 8. The mark (-) represents the points for the version with the GG while the mark (+) represents points for the version without the GG.

In Fig. 8 we see that the fan with the GG produces a smaller flow at the same static pressure difference because the net represents a resistance to airflow. From the maximum flow with the difference of 4.2%, the difference of flows is decreasing with the flow reduction as the flow pressure loss on the protective grid is falling, except for the medium area where the difference increases. Further, a distinctive difference can be established when comparing the efficiencies where the difference is significantly bigger in higher flows. The increase in deviations in the area of the optimal working point and its movement in the direction of the increased airflow volume in the case of the fan without the GG is the result of the impact of the GG on the kinematics of the flow from the fan.

The results of numeric calculations of the IC with and without the GG in the three operating areas marked in the diagram are virtually the same. In both cases, the calculated points are located very near the measured characteristic of the fan without the GG. This leads to the conclusion that the GG's impact is inadequately evaluated in integral results of the numeric model, and that the model does not include all the flow characteristics on the coaxial supporters of the net.

Fig. 8 presents the dependence of the connecting electrical power on the airflow volume on the fan. Flow $P_{el}(q_V)$ is related to the integral aerodynamic characteristic $\Delta p(q_V)$ and $\eta(q_V)$, Figure 9. The measurement results point to the division of the entire operating area in four parts. The first part between 2000 and 3600 m^3/h, where the efficiency of both fans is very similar with a difference in power consumption which increases with an increased flow and is smaller in the fan with the net as it provides for smaller flows. The second part between 3600 and 6000 m^3/h is where the difference between both efficiencies as well as the flow begin to increase. However, the difference between the power consumption levels starts to fall. The third part between 6000 and 7600 m^3/h is where the difference between the efficiencies partly falls, yet both fans consume similar power. And the last, fourth part between 7600 m^3/h and $q_{V,max}$ is where the difference between efficiency again increases but the difference between power consumption at an identical flow decreases.

This division was used as the basis for selecting three working points of the fan pertaining to individual parts. We expect to find the described characteristics to be the result of the flow kinematics and distinctly differing structures of the velocity field at the fan's outlet to be present at the selected points.

Figure 8 presents the selected points A, B and C in which measurements of the velocity field were performed as described in Section 2.2.

1.2 Local Characteristics of the Flow Field

Diagrams Figs. 10 to 15 present the results of the local characteristics. They are given in the form of a velocity distribution in the meridian plane in dependence on the selected working point (A, B and C; Fig. 8) and the position of the five-hole probe R in the radial direction from the hub to the external housing of the fan.

Presented are the measured values (the dotted line) and numerically modelled values of the velocity (the full line) of the fans with and without the GG for individual working points. Absolute velocity curves are marked as full circles, the axial components of the velocity vector with full triangles, the tangential components of the velocity vector with crosses

and the radial components of the velocity vector with empty circles, depending on the selected operating point.

Marks in the charts Figs. 10 to 12:

- Va CFD bm: Numerically calculated axial velocity of the fan without the GG;
- Va mer bm: Measured axial velocity of the fan without the GG;
- Vt CFD bm: Numerically calculated tangential velocity of the fan without the GG;
- Vt mer bm: Measured tangential velocity of the fan without the GG;
- Vr CFD bm: Numerically calculated radial velocity of the fan without the GG;
- Vr mer bm: Measured axial velocity of the fan without the GG;
- Vabs CFD bm: Numerically calculated absolute velocity of the fan without the GG and
- Vabs mer bm: Measured absolute velocity of the fan without the GG;

and for the charts in Figure 13 to Figure 15:

- Va CFD zm: Numerically calculated axial velocity of the fan with the GG;
- Va mer zm: Measured axial velocity of the fan with the GG;
- Vt CFD zm: Numerically calculated tangential velocity of the fan with the GG;
- Vt mer zm: Measured tangential velocity of the fan with the GG;
- Vr CFD zm: Numerically calculated radial velocity of the fan with the GG;
- Vr mer zm: Measured axial velocity of the fan with the GG;
- Vabs CFD zm: Numerically calculated absolute velocity of the fan with the GG and
- Vabs mer zm: Measured absolute velocity of the fan with the GG.

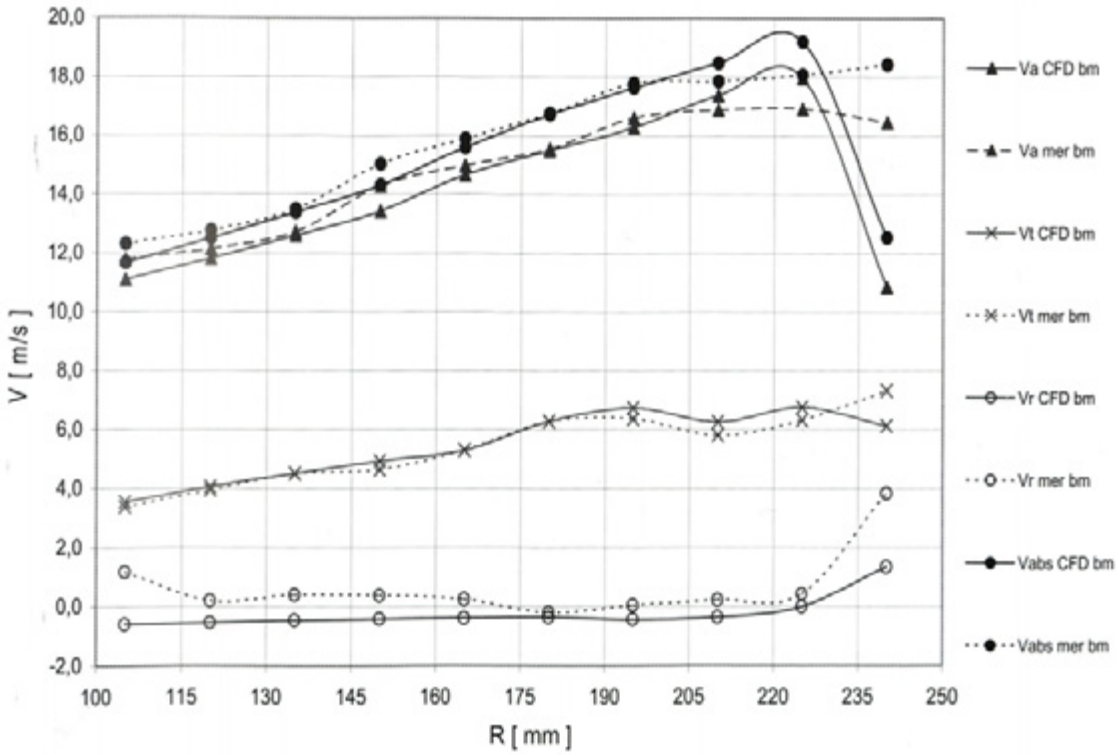

Fig.10. *Local velocities of fan without the guard grill at operating point*

The comparison between the measured and calculated components of the velocity vector at working point A shows an excellent match between the results as regards the fans with and without the GG, Figs. 10 and 13. In both cases, the axial component of the velocity vector increases linearly with the radius – position of the measuring probe, equally in both versions (with and without the GG) its value is reduced at the circumference, which is the result of the impact of the boundary layer and impact of the gap between the blade and outlet.

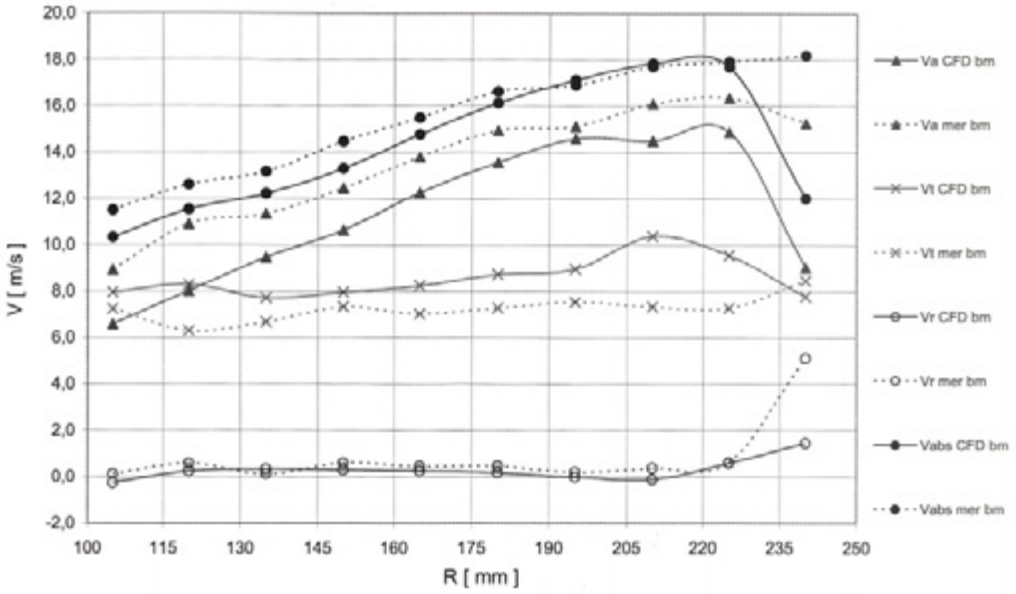

Fig. 11. *Local velocities of fan without the guard grill at operating point*

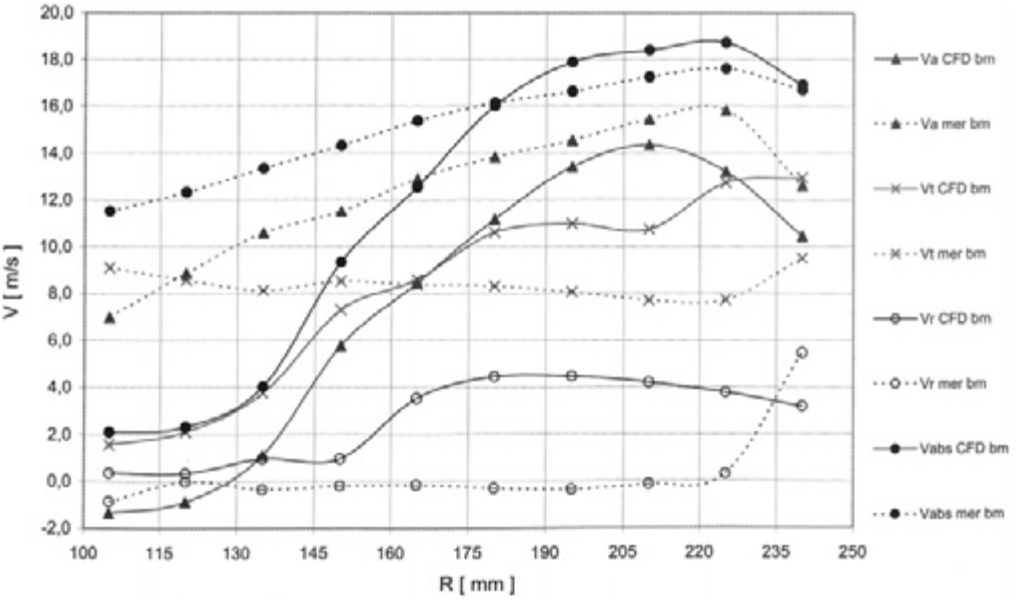

Fig.12. *Local velocities of fan without the guard grill at operating point C*

The differences between the measured absolute and modelled velocity in the area near the outlet of the fan are bigger in the case of the free outflow without the GG. These differences can be linked to deviations of measured values of the radial component of velocity for both versions of the fans and the pertaining modelled values. In the area around the housing there is a trend of an increase in the radial component of the velocity, which is more prominent in the measured values, leading to the conclusion that the flow is directed diagonally in the peripheral area.

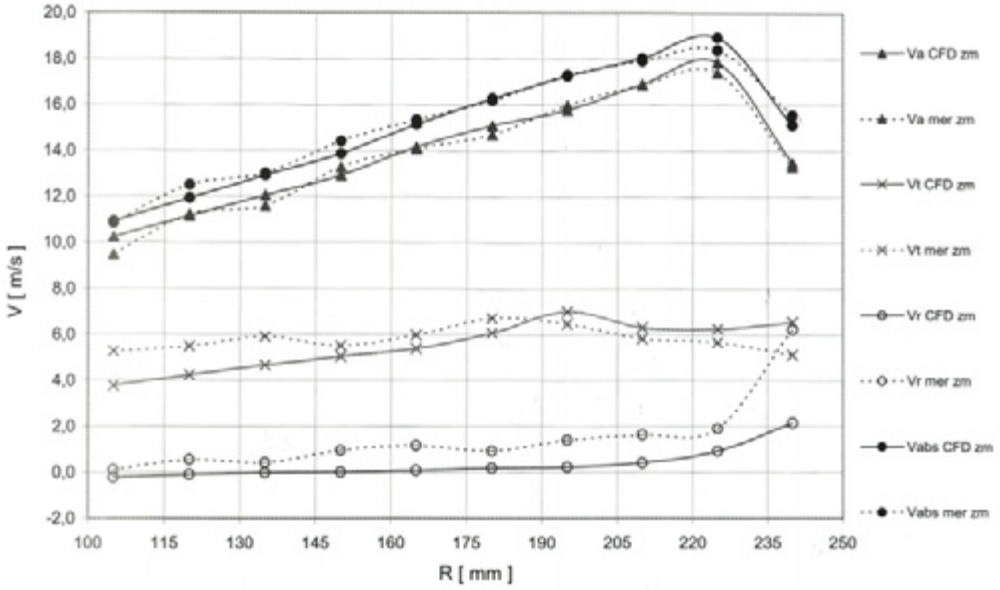

Fig. 13. *Local velocities of fan with the guard grill at operating point A*

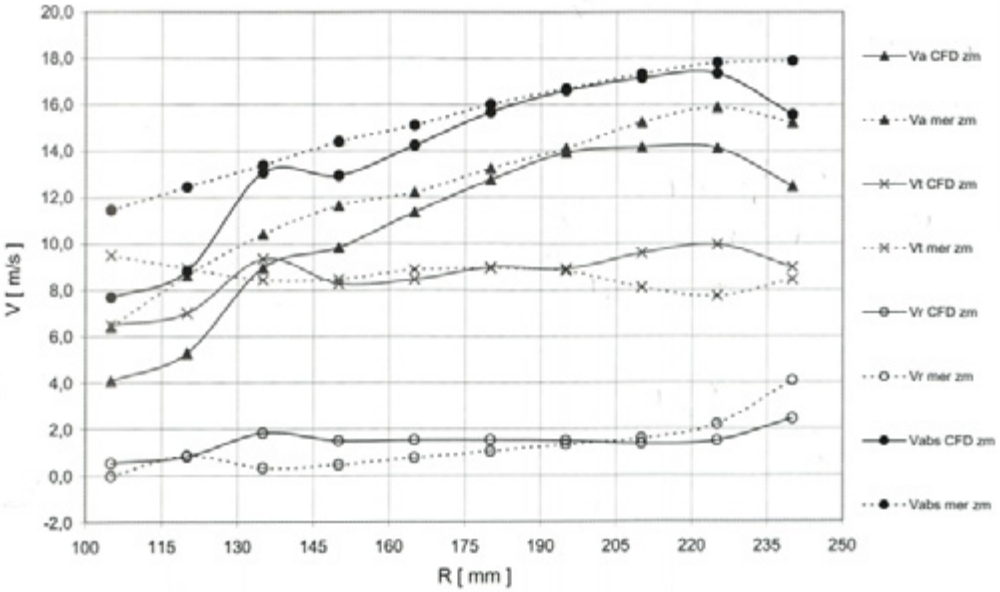

Fig. 14. *Local velocities of fan with the guard grill at operating point B*

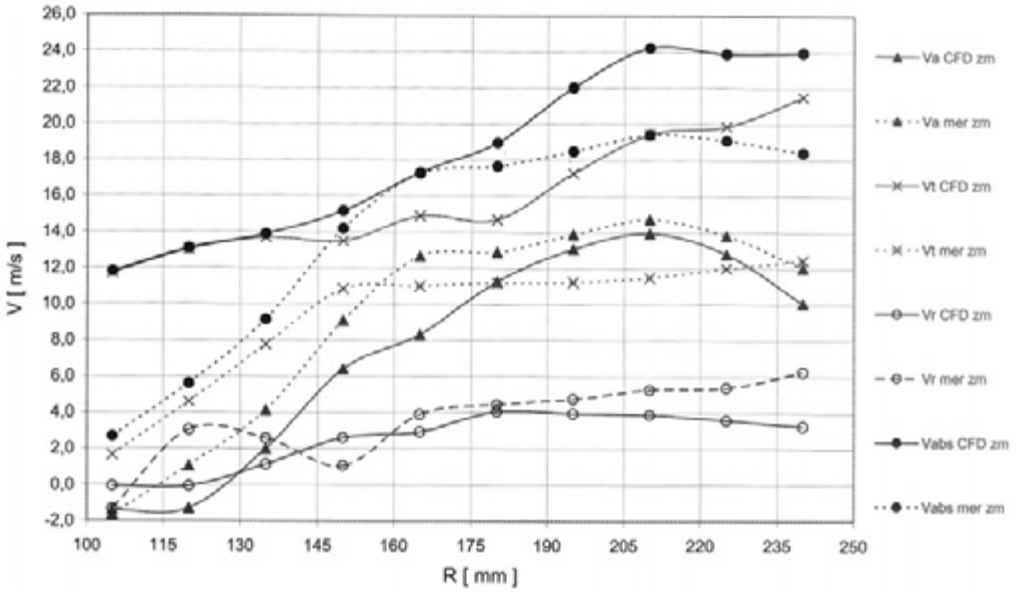

Fig. 15. *Local velocities of fan with the guard grill at operating point C*

It is a familiar phenomenon resulting from the swirl of the flow and the related centrifugal forces [1] and [2]. At point A there is a minimal difference between the components of the tangential velocity for both versions of the fans and a relatively good match with the results of the numeric model. There is an increase in the tangential component of the velocity, which is line with the expectations [1] and [2].

The differences between both versions increase at working point B, as evident from Figs. 11 and 14. By comparing the absolute velocities we can find that the trend of increasing velocity accelerates with radius R in the entire measurement area. The distinct reduction in velocity on the fan's circumference does not appear in measured values. However, it is present on the curve presenting the modelled velocity values. At this working point and as opposed to working point A there is bigger difference between the measured and modelled axial component of velocity. The match between the measured and modelled values is also poorer in the tangential component of velocity, while in both versions of the fan there is a distinct increase in the tangential component of the velocity vector, which is in line with the literature [1] and [2] and a decrease in the axial component of the velocity vector resulting from the smaller flow. A comparison with the results for working point A shows a significant increase in the radial component of the velocity vector at the circumference which is the result of an increase in the tangential component of the velocity vector.

The trend of growing differences between the modelled and measured values increases with transition to working point C. The measurement uncertainty was greater at this point due to the smaller velocities and unregulated flow which should be taken into account in the analysis of results. For both fans, the numeric calculation showed the occurrence of a backflow in the form of a negative component of the axial velocity on the circumference which was confirmed by the measurements of the fan with the GG, Fig. 15. In comparison with the previous two working points, there is a strong increase in the tangential component of the velocity vector due to the bigger produced pressure, which is greater in the fan with the GG as the airflow has less interaction with the surroundings because of the additional GG. A significant increase in comparison with the previous measurements is also in the radial component of the velocity resulting from the increase in the tangential velocity.

The analysis of local velocities together with the integral measurements yielded the

following results for the individual operating points. In the fourth part, the GG primarily affects the size of the velocity field while no change in direction occurs. This is reflected in the IC with an almost parallel efficiency-flow curve and pressure-flow curve. The almost identical direction of the velocity field is presented in Figs. 10 and 13. As regards the fan with the GG, the trend in velocity is the same as in the fan without the GG, only it is significantly smaller. The GG affects both the size and direction of the velocity field at the third operating point, Figs. 11 and 14. The impact on the change in the direction of the velocity field is reflected in the increasing difference between the pressure-flow and efficiency-flow curves, Fig. 8, reaching the biggest difference exactly as the part ends. Around this point, the impact of the GG on the IC starts to decrease while the impact on the direction of the flow field is substantial, Figs. 12 and 15.

2 CONCLUSIONS

On the basis of the presented results, we may conclude as follows:

(1) GG has a distinct impact on the aerodynamic properties of the AF. In addition to the aerodynamic resistance present due to the flow around the GG structure, impacts of the change in the velocity field should also be taken into account that form because of the effect of the geometry of the structure of the GG on the outflow from the fan's rotor.

(2) By further development it is necessary to adjust the GG to the optimal on-flow velocity field from the fan without the GG to the meshed structure for decreasing the aerodynamic resistance and increasing the efficiency in the optimal working range.

(3) Given the discrepancy between the model results and the measured values at the integral and local level, we can conclude that the GG has a distinct impact and should be included in the modelling of flow conditions on the fans. More attention should be paid to local phenomena in the flows around the GG.

(4) Experimental measurements of the velocity field have a very good match with the numeric calculations in the operating area of the AF. However, as the difference of the static pressure of the AF increases the irregularity of the flow rises and so the uncertainty in measuring the velocity field with a five-hole probe and in the numeric calculation grows.

3 REFERENCES

[1] Wallis, R. A. (1983) Axial flow fans and ducts; *John Wiley & Sons*.

[2] Eck, B. (1973) Fans; Design and operation of centrifugal, axial-flow and cross-flow fans; *Perganom press Ltd., Headington Hill Hall*, Oxford.

[3] Eck,B.(1978) Technische Strromungslehre; *Springer Verlag*; Berlin Heidelberg New York.

[4] Li, Y. (2007) Experimental research on aerodynamic performance and exit flow field of low-pressure axial flow fan with circumferential skewed blades; *Journal of Hydrodinamics*.

[5] Kergourlay, G. Koudri, S., Rankin G. W., Rey R. (2006) Eksperimental investigation of the 3D unsteady flow field of axial fans; *Flow measurements and instrumentation*.

[6] Abdel-Rahman, A. A., Chakroun, W., Al-Fahed S. F, (1997) LDA measurements in the turbulent round jet; *Mechanics research comunications*.

[7] Corsini, A., Rispoli F.(2005) Flow analyses in a high-presure axial fan with a non-linear eddy-viscosity closure, *Heat and fluid flow*.

[8] Oh, K-J., Kang, S-H.(1999) A numerical investigation of th,e dual performance characteristics of a small propeller fan using viscosius flow calculations, *Computers&fluids*.

[9] Estevadeordal, J., Gogineni, S., Copenhawer, W., Bloch, G., Brendel, M.(2000) Flow field in a low-velocity axial fan: a DPIV investigation; *Experimental thermal and fluid science*.

[10] Yoon, J-H., Lee S-J.(2004) Stereoscopic PIV measurements of flow behind an isolated low-velocity axial fan; *Experimental thermal and fluid science*.

[11] International organization for standardization; Industiral fans –

Performance testing using standardized airways, ISO 5801,(1997).

[12] Nobusuke, H., Naoki, S., Shigehisa, F. (2001) Outdoor unit of air condetioner JP2003172528; *European patent office*.

[13] Toshiya, F. (2003) Fan grill and outdoor equipment for air-conditioner JP2003172528; *European patent office*.

[14] Wilhelmus, E. (2004) Outlet grill for use in an air-blowing device having axial fan WO200406839; *European patent office*.

[15] Chondrokostas, C. (2005) Calibration of pneumatic five-hole probes in the free-jet wind tunel; *Tehnische Universitaet Wien*.

[16] Zilliac, G.G. (1989) Calibration of seven-hole pressure probes for use in fluid flows with large angularity; *NASA*.

[17] Dugao, Z., Jing, Z., Juan, S. (1996) Optimization design of an axial flow fan used for mining local ventilation, *Computers ind. Engng*.